



Measurement-induced quantum phases realized in a trapped-ion quantum computer

Crystal Noel^{1,2,3}✉, Pradeep Niroula^{1,4}, Daiwei Zhu¹, Andrew Risinger¹, Laird Egan¹, Debopriyo Biswas¹, Marko Cetina^{1,2}, Alexey V. Gorshkov^{1,4}, Michael J. Gullans⁴, David A. Huse⁵ and Christopher Monroe^{1,2,3,4,6}

Many-body open quantum systems balance internal dynamics against decoherence and measurements induced by interactions with an environment^{1,2}. Quantum circuits composed of random unitary gates with interspersed projective measurements represent a minimal model to study the balance between unitary dynamics and measurement processes^{3–5}. As the measurement rate is varied, a purification phase transition is predicted to emerge at a critical point akin to a fault-tolerant threshold⁶. Here we explore this purification transition with random quantum circuits implemented on a trapped-ion quantum computer. We probe the pure phase, where the system is rapidly projected to a pure state conditioned on the measurement outcomes, and the mixed or coding phase, where the initial state becomes partially encoded into a quantum error correcting codespace that keeps the memory of initial conditions for long times^{6,7}. We find experimental evidence of the two phases and show numerically that, with modest system scaling, critical properties of the transition emerge.

An isolated many-body quantum system undergoes unitary evolution until it is probed by its environment via quantum measurement^{1,2}. The irreversible process of measurement converts quantum coherence in the system into classical entropy in the measurement apparatus due to the intrinsic randomness of quantum measurements. When the rate of partial measurements is high, this process ‘collapses’ the many-body system into a pure quantum state consisting of locally correlated regions determined by the recent unitary dynamics and measurement outcomes. At low measurement rates, however, there is a mixed (coding) phase where the associated projections can leave invariant a codespace in the system that retains memory of the initial conditions for exponentially long times^{6,7}. Such measurement-induced phase transitions have recently been theoretically explored in models based on random quantum circuits^{3–7}, but are believed to be a ubiquitous phenomenon in monitored non-equilibrium quantum systems. The theory of these transitions, although still nascent, has seemingly deep connections to percolation and conformal field theory^{3,5,8,9}, as well as threshold theorems in fault-tolerant quantum computing^{10,11}. Observing these effects in experiments is a formidable challenge because measuring the observables that signify the transition requires exquisite control and isolation of the system, accurate monitoring by an external measurement apparatus, and the use of sophisticated feedback or post-processing with the measurement data.

In this Letter we report on a direct experimental observation of the two phases associated with a measurement-induced purification transition in a trapped-ion quantum computer. We use a single reference qubit initially entangled with the system to directly test for the existence of the codespace in the mixed phase and its absence in the pure phase¹². This approach has the practical benefit that it relaxes experimental resource requirements compared to observables that require measuring entanglement entropies of large numbers of qubits, such as measuring Renyi entropy¹³. We avoid the use of post-selection on measurement outcomes through the addition of feedback operations that reverse any measurement-induced unitary rotations on the reference qubit (so-called ‘quantum steering’ effects¹⁴). As a result, absent noise, our experimental approach is directly scalable to large systems.

From early measurements of the quantum-to-classical nature of measurement in ion-trap systems¹⁵ and cavity quantum electrodynamics¹⁶, to the recent observation of wavefunction collapse in superconducting qubits¹⁷, the phenomenon of measurement itself has been a subject of great interest experimentally. Many-body coherent operations combined with controlled dissipation or measurements have been explored experimentally in, for example, the study of dissipative state preparation¹⁸, as well as in recent theoretical proposals for many-body quantum non-demolition measurements¹⁹. We also note related experimental results showing symmetry-resolved dynamical purification of spin chains in a long-range XX model with local depolarizing noise^{13,20}. By contrast, in our study, we employ a ‘digital’ model of computing with two-site unitaries and projective measurements with a temporal randomness to the dynamics.

Our quantum computer uses up to 13 $^{171}\text{Yb}^+$ qubits in a single chain of 15 trapped ions in a microfabricated chip trap²¹. We achieve a universal gate set with native single-qubit gate fidelities of 99.96% and two-qubit gate fidelities on any pair of 98.5–99.3%, as detailed elsewhere²².

We now describe the specific dynamics of the random circuits in this work with a system of L qubits subject to unitary evolution with all-to-all connectivity and measurements. For such all-to-all coupled models, spatial entanglement of the wavefunction is not a reliable diagnosis of the measurement-induced phase transition; instead we characterize the problem in terms of a purification transition⁶. In this picture, the system transitions at low measurement rates to a phase with long-range correlations in time, similar to the behaviour found in fault-tolerant error-correction thresholds.

¹Joint Quantum Institute, Departments of Physics and Electrical and Computer Engineering, NIST/University of Maryland, College Park, MD, USA. ²Duke Quantum Center and Department of Physics, Duke University, Durham, NC, USA. ³Department of Electrical and Computer Engineering, Duke University, Durham, NC, USA. ⁴Joint Center for Quantum Information and Computer Science, NIST/University of Maryland, College Park, MD, USA. ⁵Department of Physics, Princeton University, Princeton, NJ, USA. ⁶IonQ, Inc., College Park, MD, USA. [✉]e-mail: crystal.noel@duke.edu

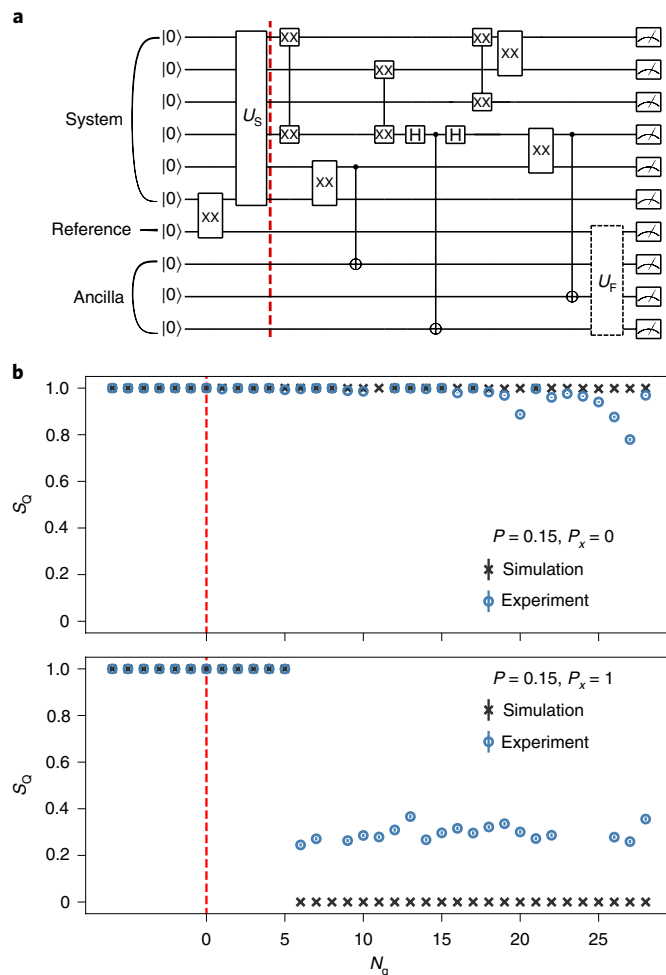


Fig. 1 | Model and purification dynamics. **a**, Schematic of a circuit with $L=6$ system qubits, $N_g=6$ two-qubit gates, two z measurements and one x measurement. The first XX gate entangles the reference with a system qubit. Next, we scramble the system, U_s . The time evolution of the unitary-measurement dynamics starts at the red dashed line. Probabilistic measurement is deferred until the end of the circuit using CNOT gates between system qubits and measurement ancillae. The x -basis measurement is shown after the third XX gate. Finally, a feedback operation U_f is applied (Methods and Extended Data Fig. 3). **b**, The entropy of the reference qubit for two $L=6$ circuits where the reference qubit stays mixed (upper panel) and purifies (lower panel). The x axis shows the evolution of time in units of applied two-qubit gates (N_g) after scrambling is complete (indicated again by the red dashed line). In this example, the entropy is measured by performing single-qubit tomography of the reference by making measurements in the x , y and z bases. Error bars (1σ) are smaller than the markers, with 4,000 and 10,000 shots for experiment and simulation, respectively. Missing experiment data are due to ion loss events, which are assumed to be uncorrelated with the data being taken.

This dynamical purification phase transition can be efficiently probed by studying how the system preserves entanglement over time with a single reference qubit¹².

An example circuit is shown in Fig. 1a. After preparing all qubits in $|0\rangle$, the reference is entangled to a randomly selected system qubit to form a Bell pair. The entangling operation is followed by a scrambling unitary, which consists of random single-qubit Clifford gates and two-qubit $XX(\pi/4)$ gates on random qubit pairs. The scrambling stage spreads the entanglement to the entire system and reduces finite-size effects (Methods and Extended Data

Fig. 1). After scrambling the system qubits, we evolve the system in time with random unitary dynamics and measurements with a total number $N_g = \lfloor L\sqrt{L} \rfloor$ of $XX(\pi/4)$ gates applied to randomly chosen qubit pairs.

After each entangling gate we add a measurement with probability P (Methods). Although mid-circuit readout of ion qubits is possible²³, we use ancilla qubits to defer readout. When a circuit calls for measurement, we entangle that qubit with an ancilla in a chosen measurement basis. Because the unitaries are XX gates, the measurement choice of the z or x basis has a strong effect on the subsequent dynamics. This feature of our model allows us to tune the probability, P_x , that a measurement is in the x basis to go across the purification transition without directly changing P . At the end of the circuit, all the qubits are read out in the z basis via fluorescence imaging. For each circuit, we rotate the reference qubit to measure in x , y and z bases and post-select the observations to obtain Pauli expectations conditioned on measurement outcomes (Methods and Extended Data Fig. 2). The set of three Pauli expectations are then used to construct the density matrix of the reference qubit and measure its entropy S_Q . These circuits are examples of stabilizer circuits, whose noiseless dynamics are classically simulable^{24,25}.

As an illustrative example, in Fig. 1b we consider the experimentally measured evolution of S_Q in two circuits sampled from ensembles with $P=0.15$. We choose one circuit sampled from $P_x=0$ that stays mixed (encoded) and one sampled from $P_x=1$ that purifies over time. Units of time are measured in the number of applied two-qubit gates, N_g , for consistency between theory and experiment. For noiseless stabilizer circuits, the entropy is always either 0 or 1 bit²⁵ and, as a result, the circuits that purify must do so at precisely one time step. However, this property no longer holds exactly in the presence of noise. Experimentally, we find that the mixed circuit maintains a high value of S_Q . In the second circuit, the reference qubit purifies at the expected time in the circuit, albeit to a constant offset due to experimental noise. It is apparent from these examples that we observe a clear separation between pure and mixed results for S_Q . For each circuit, we ran 4,000 shots of each measurement basis (x , y , z) to compute S_Q at each time step.

To characterize the many-body dynamics, we generated large ensembles of circuits and averaged their entropy for given values of P , P_x and L . In Fig. 2a we show the theoretical phase diagram for the model versus P and P_x . For low P and P_x , the system is driven to a mixed (coding) phase where the non-unitary dynamics projects quantum information about the initial state into a random quantum error correcting code. As either P or P_x is increased, the system enters a pure phase, where an initial mixed state collapses to a fixed quantum state and the encoding operation fails. The behaviour at $P=0$ can be smoothly connected to the finite P behaviour by scaling N_g by $1/P$ and taking the limit $P \rightarrow 0$. In this limit, there is residual purification dynamics that leads to a phase transition along the $P=0^+$ axis. This special critical point arises because of the restricted nature of our gates, which do not effectively scramble the system in the absence of measurements²⁶. The critical point at each value of P was obtained from finite-size scaling analysis using simulations of $L=16$ to $L=64$ qubits (Methods). Our scaling analysis is based on extracting the exponential decay rate of $\langle S_Q(t) \rangle$ at late times.

In Fig. 2b we show the simulated dynamics of $\langle S_Q(t) \rangle$ at two representative points in the phase diagram with $P=0.15$. In the mixed phase, probed at $P_x=0$, $\langle S_Q \rangle$ stays near one for exponentially long times in L . Deep in the pure phase, the reference qubit rapidly purifies, with an average entropy that exponentially approaches zero. In the experiment, we probe small systems $L \leq 8$ after a number $L^{1.5}$ of gate operations. For larger numbers of qubits L , this scaling limit is sufficient to probe the phase because the effective depth of the circuit scales as $2\sqrt{L}$, much greater than any fixed correlation time in the system. At the critical point, as we show in Extended Data Fig. 6,

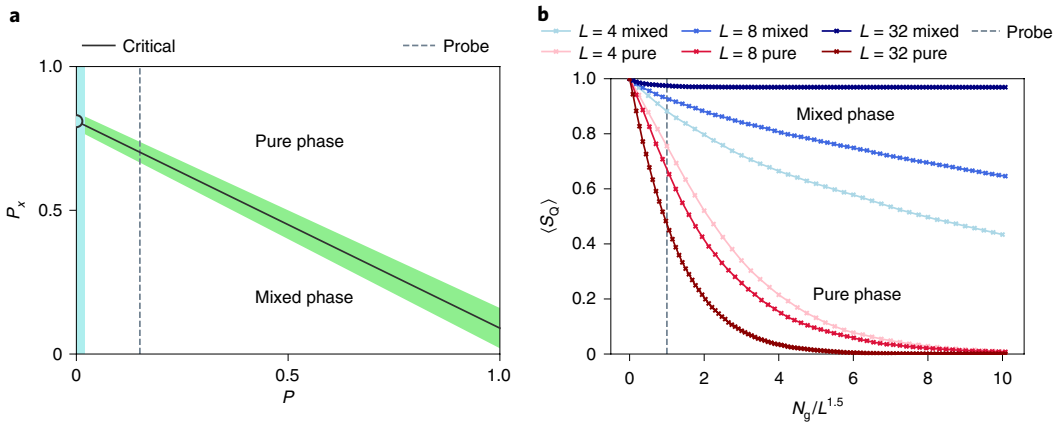


Fig. 2 | Phase diagram and scaling limit of average purification dynamics. **a**, The phase diagram of the model, parameterized by P and P_x . The green shaded region indicates the numerical uncertainty in the critical region between the top phase, where the reference qubit rapidly purifies, and the bottom phase, where it stays mixed. In our experiment, we fix $P=0.15$, and tune P_x to probe the phase transition along the dashed line. In the limit $P \rightarrow 0$ (left blue shaded region) with N_g also scaled as $1/P$, the restricted nature of our gate ensemble leads to a purification transition (circle) when tuning P_x along the line $P=0^+$. **b**, The simulated entropy of the reference qubit averaged over many random circuits $\langle S_Q \rangle$ in the two phases. Here we use the same fixed value of $P=0.15$ from A, with $P_x=0$ (mixed) and $P_x=1$ (pure) plotted against time (measured in units of two-qubit gates) scaled by $L^{1.5}$. The dashed vertical line indicates the experimental probe time of $N_g=L^{1.5}$, and the intersection of this line with different system sizes shows increasing (decreasing) entropy in the mixed (pure) phase that is the signature of the two phases.

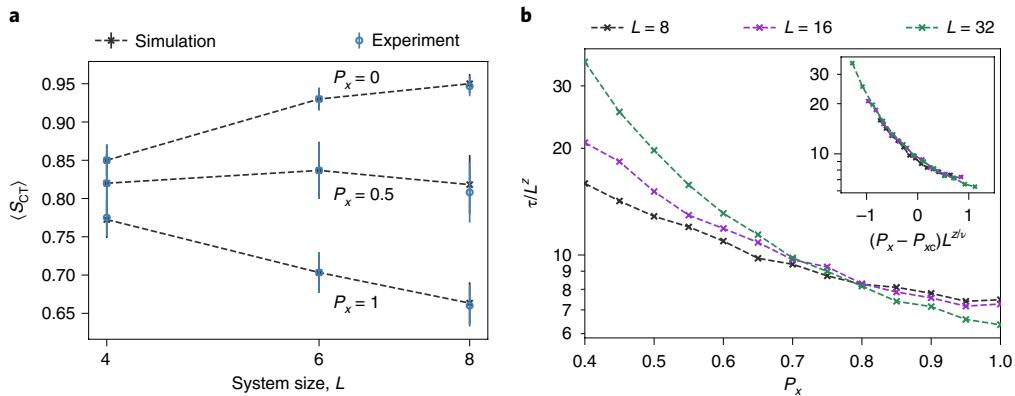


Fig. 3 | Experimental observation of phases and simulated critical behaviour. **a**, Classical entropy after thresholding $\langle S_{CT} \rangle$, averaged over an ensemble of random circuits at varying system sizes. We show evidence of mixed (top), intermediate (middle) and pure (bottom) phase, with $P_x=0$, $P_x=0.5$ and $P_x=1$, respectively, and with size scaling as predicted in Fig. 2b. Error bars are 1σ uncertainty with 300 circuits for $P_x=0, 1$ and with 100 circuits for $P_x=0.5$. **b**, Simulated results showing the late-time decay rate τ of $\langle S_Q \rangle$ near the transition. $z \approx 1/5$ is the dynamical critical exponent, $\nu \approx 1/2$ is the correlation length exponent and $P_{xc}=0.72(1)$ is the critical value of P_x . These critical parameters are extracted from a finite-size scaling analysis (Methods and Extended Data Fig. 6).

the entropy decay time scales as $L^{1/5}$ to conform to the universal critical dynamics of the system.

To reduce the number of circuits needed to evaluate S_Q , we append a feedback circuit to the end of each circuit that is expected to purify. The feedback uses single-qubit rotations and a circuit of CNOT gates between the reference and measurement ancillae to disentangle it from the measurement ancillae (Methods). With this addition, we replace measurement of S_Q with the classical entropy S_C , and eliminate the need to measure in the x basis and y basis. This feedback approach avoids post-selection and remains tractable for stabilizer circuits on any system size because we can efficiently find the feedback circuit²⁴. Finding efficient extensions of this feedback approach for arbitrary gate sets and circuit architectures is an unsolved problem¹². Many of the naive approaches to investigating the phase transition for random circuit ensembles with a universal gate set requires some form of post-selection on the measurement outcomes. It is therefore an important goal to develop efficient

feedback protocols (or other methods to circumvent post-selection) for generic random circuit models. Alternatively, it may be possible in some cases to give complexity theoretic evidence that an efficient feedback protocol does not exist.

To probe the phases experimentally, we generate an ensemble of random circuits for the chosen values of P , P_x and L . To constrain the number of measurements to a low value, we study a fixed line of parameters at $P=0.15$ (Fig. 2a), and the evolution is applied for a time N_g . At the end of the circuit, we measure the reference in the z basis. We average over many shots to determine S_C for each circuit. The majority of experimental noise can be explained with a simple noise model using XX-gate crosstalk (see the Supplementary Information, where we also describe techniques to further mitigate errors). We assume a Gaussian distribution of expected $S_C=0$ circuit outcomes and $S_C=1$ circuit outcomes and find their intersection, which is used as a threshold at $S_C=0.93$ (Extended Data Figs. 4 and 5). Any outcome below the threshold is counted as $S_{CT}=0$,

and those above as $S_{\text{CT}} = 1$. For $P_x = 0, 1$ ($P_x = 0.5$), we average the entropy after binning with the threshold, $\langle S_{\text{CT}} \rangle$, over the results of 300 (100) unique circuits.

We study $\langle S_{\text{CT}} \rangle$ at $P_x = (0, 0.5, 1)$ and $L = (4, 6, 8)$, and observe the first experimental evidence of the phases of a dynamical purification phase transition. Although the measured entropy increases with system size in the mixed phase ($P_x = 0$), in the pure phase ($P_x = 1$), the entropy decreases with system size (Fig. 3a). This behaviour is expected and can readily be seen in simulations at the experimental probe time in the example in Fig. 2b. To probe the crossover behaviour on these system sizes, we also sample at an intermediate value of $P_x = 0.5$ close (for these sizes) to the critical point at $P_{xc} = 0.72(1)$. We observe consistent results with the simulations in this near-critical regime, showing behaviour that interpolates between the two extremes.

Having obtained conclusive evidence for the two phases in our system, it remains an outstanding challenge to experimentally probe the universal critical behaviour of this model. We predict that such effects will become accessible in our system through modest increases in system sizes from $L = 8$ to $L = 32$ qubits, combined with periodic sympathetic cooling²⁷, which enables mid-circuit measurements, improves fidelities at late times, and should allow for deeper circuits. We have found that a sensitive probe of the critical properties of the purification transition is the late-time exponential decay constant τ of the order parameter $\langle S_Q(t) \rangle \sim e^{-t/\tau}$. Figure 3b shows an example of a finite-size scaling analysis that can be used to extract critical properties of the model. Here we use direct simulations of the ideal circuit evolution to predict the behaviour of our system as it is scaled to larger sizes. Crucially, these scaling results illustrate that the critical properties of the purification transition are obtainable using the modest system sizes and circuit depths accessible in near-term ion-trap hardware.

Our results show that measurement-induced quantum phases are accessible in near-term quantum computing systems, despite the formidable experimental challenges. Recent years have seen a host of advances in mapping out the phenomenology of these novel non-equilibrium phases of matter, including the prediction of topological order stabilized by measurements in random circuits^{26,28,29} and applications in computational complexity theory³⁰ and quantum error correction³¹. These developments point to a broad potential for the advancement of many-body physics and quantum information science through the continued explorations of quantum measurement.

From the perspective of fault-tolerant quantum computation, our results open up a number of new directions. Investigating similar physics in fault-tolerant operating regimes with error correction and feedback built into the model is an exciting direction for future work. Although the resource demands are often difficult to satisfy for fault-tolerant simulations, the intrinsic flexibility in implementing random circuit models allows one to circumvent the worst-case behaviour analysed in fault-tolerant threshold theorems¹¹. As a result, many of the resource costs for fault tolerance can be lowered for random circuits. For example, much of the overhead in the standard models for fault tolerance arises from implementing a universal gate set. We have shown that measurement-induced phase transitions are experimentally accessible with discrete gate sets, like the Clifford group, which have efficient fault-tolerant transversal implementations in systems with long-range interactions, such as ion traps. Additional gates outside this set can be introduced with a low density to avoid a large increase in the overhead for more generic random circuit models.

An important conceptual aspect of our work is that we experimentally study an error-correction threshold as a physical phenomenon, exploring its connections to universality in quantum many-body physics. This approach contrasts with many earlier works on experimental quantum error correction that have so far

focused primarily on demonstrations of few-body gadgets in the below-threshold regime²². In addition, although error-correction thresholds can be studied numerically, applying those theories in practice requires a deeper understanding of the errors in real physical systems, and how the corresponding thresholds behave. The ability to successfully operate quantum computing systems in these near-critical regimes is likely to be a crucial aspect in the future of fault-tolerant quantum computing.

Online content

Any methods, additional references, Nature Research reporting summaries, source data, extended data, supplementary information, acknowledgements, peer review information; details of author contributions and competing interests; and statements of data and code availability are available at <https://doi.org/10.1038/s41567-022-01619-7>.

Received: 14 October 2021; Accepted: 26 April 2022;

Published online: 02 June 2022

References

1. Carmichael, H. *An Open Systems Approach to Quantum Optics* (Springer, 1993).
2. Gardiner, C. W. & Zoller, P. *Quantum Noise* (Springer, 2000).
3. Skinner, B., Ruhman, J. & Nahum, A. Measurement-induced phase transitions in the dynamics of entanglement. *Phys. Rev. X* **9**, 031009 (2019).
4. Li, Y., Chen, X. & Fisher, M. P. A. Quantum Zeno effect and the many-body entanglement transition. *Phys. Rev. B* **98**, 205136 (2018).
5. Li, Y., Chen, X. & Fisher, M. P. A. Measurement-driven entanglement transition in hybrid quantum circuits. *Phys. Rev. B* **100**, 134306 (2019).
6. Gullans, M. J. & Huse, D. A. Dynamical purification phase transition induced by quantum measurements. *Phys. Rev. X* **10**, 041020 (2020).
7. Choi, S., Bao, Y., Qi, X.-L. & Altman, E. Quantum error correction in scrambling dynamics and measurement-induced phase transition. *Phys. Rev. Lett.* **125**, 030505 (2020).
8. Jian, C.-M., You, Y.-Z., Vasseur, R. & Ludwig, A. W. W. Measurement-induced criticality in random quantum circuits. *Phys. Rev. B* **101**, 104302 (2020).
9. Bao, Y., Choi, S. & Altman, E. Theory of the phase transition in random unitary circuits with measurements. *Phys. Rev. B* **101**, 104301 (2020).
10. Aharonov, D. Quantum to classical phase transition in noisy quantum computers. *Phys. Rev. A* **62**, 062311 (2000).
11. Gottesman, D. An introduction to quantum error correction and fault-tolerant quantum computation. *Quant. Info. Sci. Contr. Math., Proc. Symp. App. Math.* **68**, pp.13–58 (Amer. Math. Soc., Providence, Rhode Island, 2010).
12. Gullans, M. J. & Huse, D. A. Scalable probes of measurement-induced criticality. *Phys. Rev. Lett.* **125**, 070606 (2020).
13. Brydges, T. et al. Probing Rényi entanglement entropy via randomized measurements. *Science* **364**, 260–263 (2019).
14. Schrödinger, E. Probability relations between separated systems. *Math. Proc. Camb. Philos. Soc.* **32**, 446–452 (1936).
15. Wineland, D. J. Nobel lecture: Superposition, entanglement and raising Schrödinger's cat. *Rev. Mod. Phys.* **85**, 1103–1114 (2013).
16. Haroche, S. Nobel lecture: Controlling photons in a box and exploring the quantum to classical boundary. *Rev. Mod. Phys.* **85**, 1083–1102 (2013).
17. Minev, Z. K. et al. To catch and reverse a quantum jump mid-flight. *Nature* **570**, 200–204 (2019).
18. Barreiro, J. T. et al. An open-system quantum simulator with trapped ions. *Nature* **470**, 486–491 (2011).
19. Yang, D., Grankin, A., Sieberer, L. M., Vasilyev, D. V. & Zoller, P. Quantum non-demolition measurement of a many-body Hamiltonian. *Nat. Commun.* **11**, 775 (2020).
20. Vitale, V. et al. Symmetry-resolved dynamical purification in synthetic quantum matter. *SciPost Phys.* **12**, 106 (2022).
21. Maunz, P. L. W. High optical access trap 2.0. Report No. SAND2016-0796R (Sandia National Laboratories, 2016); <http://prod.sandia.gov/techlib/access-control.cgi/2016/160796r.pdf>
22. Egan, L. et al. Fault-tolerant control of an error-corrected qubit. *Nature* **598**, 281–286 (2021).
23. Foss-Feig, M. et al. Entanglement from tensor networks on a trapped-ion QCQD quantum computer. *Phys. Rev. Lett.* **128**, 150504 (2022).
24. Gottesman, D. The Heisenberg representation of quantum computers. In *Proc. XXII International Colloquium on Group Theoretical Methods in Physics* 32–43 (International Press, 1998); <https://arxiv.org/abs/quant-ph/9807006>
25. Aaronson, S. & Gottesman, D. Improved simulation of stabilizer circuits. *Phys. Rev. A* **70**, 052328 (2004).

26. Ippoliti, M., Gullans, M. J., Gopalakrishnan, S., Huse, D. A. & Khemani, V. Entanglement phase transitions in measurement-only dynamics. *Phys. Rev. X* **11**, 011030 (2021).
27. Cetina, M. et al. Control of transverse motion for quantum gates on individually addressed atomic qubits. *PRX Quantum* **3**, 010334 (2022).
28. Lavasani, A., Alavirad, Y. & Barkeshli, M. Measurement-induced topological entanglement transitions in symmetric random quantum circuits. *Nat. Phys.* **17**, 342–347 (2021).
29. Sang, S. & Hsieh, T. H. Measurement-protected quantum phases. *Phys. Rev. Res.* **3**, 023200 (2021).
30. Napp, J., La Placa, R. L., Dalzell, A. M., Brandao, F. G. S. L. & Harrow, A. W. Efficient classical simulation of random shallow 2D quantum circuits. *Phys. Rev. X* **12**, 021021 (2022).
31. Gullans, M. J., Krastanov, S., Huse, D. A., Jiang, L. & Flammia, S. T. Quantum coding with low-depth random circuits. *Phys. Rev. X* **11**, 031066 (2021).

Publisher's note Springer Nature remains neutral with regard to jurisdictional claims in published maps and institutional affiliations.

© The Author(s), under exclusive licence to Springer Nature Limited 2022

Methods

Scrambling unitary. A scrambling unitary, U_s , is applied after the system is entangled with the reference, before the random time evolution begins. The scrambling unitary consists of four layers: odd-numbered layers are composed of single-qubit operations on each qubit and even-numbered layers are composed of fully entangling $XX(\pi/4)$ gates on $L/2$ random qubit pairs.

Measurement protocol. In our circuit ensemble, each gate after the scrambling layer is followed by a probabilistic measurement. Given the constraints of the hardware, we choose a measurement strategy that reduces the number of measurements. In addition, the ensemble generated with our measurement strategy scales to system sizes that are beyond the reach of available hardware and can only be studied with numerical simulations.

We maintain a list \mathcal{M} that is initialized to all system qubits in the beginning of the circuit. After each gate, we measure one of the qubits involved in the gate with probability P . Having decided to perform a measurement after an XX gate, we randomly choose the qubit to measure and the basis of measurement. If both qubits participating in the XX gate are in \mathcal{M} , we randomly select one with probability half and measure it in the x basis with probability P_x and in the z basis with probability $1 - P_x$. If only one of the qubits is in \mathcal{M} , we measure that qubit in the x basis with probability P_x and in the z basis with probability $1 - P_x$. If neither qubit is in \mathcal{M} , we do not measure any. Measurement outcomes in Clifford circuits are deterministic or are equally likely to be zero or one. In the absence of noise, measuring a qubit with a deterministic outcome has no effect on the purification of the reference. As a result, we only measure qubits with non-deterministic outcomes. Additionally, after each physically performed measurement, we remove the measured qubit from \mathcal{M} . Once $|\mathcal{M}| = L - 4$, we reinitialize the list with all the qubits in the system. With a low measurement probability, $P = 0.15$, used in our experiment, the number of measurements in the circuits investigated is less than 4, so the list \mathcal{M} need not be reinitialized. This ensures that no system qubit in the experiment is measured more than once.

Feedback. The feedback circuit is added at the end to disentangle the reference from the ancillae qubits. In the pure phase, the reference qubit purifies in one of x , y or z bases and its state (0 or 1) depends on the projections induced upon the measurement ancillae. The basis of purification can be anticipated with classical simulation of the Clifford circuit. A single-qubit rotation is performed on the reference qubit to ensure that it returns to the z basis following purification. Because we do not have access to the measurement outcome until the very end of the circuit, we construct a logic circuit, consisting of CNOT gates, to ensure that the reference qubit purifies to the zero state. This is done by classically anticipating the entanglement between measurement ancillae and reference qubit, then generating a sequence of CNOT gates to disentangle the reference.

For example, in batch $L = 4$, $P_x = 0$, circuit #45 purifies the reference in the x basis. There are three measurements. The outcomes of the measurement ancillae and the reference qubit are related by the truth table in Extended Data Fig. 2.

The feedback circuit, in this particular case, is given by the circuit diagram in Extended Data Fig. 3. The Hadamard gate is used to align the reference along the z basis. The following sequence of CNOT and X gates implement the logic to disentangle the reference from the ancillae. When implementing the circuit, all CNOT gates are compiled to XX gates³².

Circuit optimization. For each circuit, commuting single-qubit rotations and $XX(\pi/4)$ gates are merged, wherever possible, to reduce the size of the circuit.

Raw data and thresholding. Data presented in Fig. 3a are presented after binning via a threshold. Extended Data Fig. 4 presents histograms of the outcomes for all circuits, with each entropy averaged over the outcome of 1,000 shots per circuit. Furthermore, Extended Data Fig. 5a shows the average classical entropy over all circuits for each system size and P_x value. These averages are clearly much higher than the simulations.

The primary reason for the discrepancy between the simulations and the experimental data is that the simulations do not include noise. When including realistic noise sources in the simulations ('Noise model' section in the Supplementary Information), such as dephasing or gate amplitude errors, we find that the entropy outcomes are pushed to higher values. Nevertheless, we see in the data for $L = 4$ and $L = 6$ that there is a clear separation observed in the entropy values for circuits that are mixed or pure (Supplementary Fig. 2). This separation is also evident in Fig. 1b, with the clear jump from mixed to pure in the evolution of the circuit.

We can use these properties of the circuits to mitigate noise effects. In the final data processing, we assume a Gaussian distribution of expected $S_c = 0$ and $S_c = 1$ circuit outcomes and find their intersection, which is used as a threshold at $S_c = 0.93$. Circuit outcomes below the threshold are counted as 0 and outcomes above are counted as 1. We find three thresholded circuit outcomes disagree with the simulated expected value for that circuit, for an error of 3/699 circuits for the $L = 8$ case. Extended Data Fig. 5b shows the result after all processing alongside

simulations of the exact circuits for sizes $L = (4, 6, 8)$ and representative samples for sizes $L = (16, 32)$. The same threshold is used for all system sizes.

Critical scaling theory. Our method for locating the critical point in these all-to-all models is illustrated in Extended Data Fig. 6. For $P_x \sim P_{xc}$, we can run the dynamics out to a time where $\langle S_0(t) \rangle$ exhibits a simple exponential decay $\propto e^{-t/\tau}$. We then use least-squares fitting to find the exponential decay rate τ for each value of P_x and L . Deep in the mixed phase, τ diverges exponentially with L (ref. ⁶), whereas in the pure phase τ approaches a constant independent of system size. At the critical point ($P_x = P_{xc}$), $\tau \sim L^z$, where z is the dynamical critical exponent. Thus, we can estimate P_{xc} by looking for the value of P_x where $\tau(L)$ goes through an inflection point on a log-log plot. This behaviour is illustrated in Extended Data Fig. 6b for the model with $P = 0.15$ and $|\mathcal{M}| \geq L - 4$. Near $P_x = 0.7 - 0.75$, we see that the decay rate τ grows as power law $L^{1/5}$ over the given range of sizes. This value of $z = 1/5$ is consistent with the scaling one would expect from mean-field percolation. The close ties between these phase transitions and percolation have been noted in past works. Notably, for the Hartley entropy of Haar random circuits with measurements, there is an exact mapping to a percolation problem in the circuit geometry³. In the all-to-all setting considered here, this mapping also predicts $z = 1/5$.

Using this estimate for z , we can accurately measure the critical point P_{xc} and critical exponent ν of the purification transition using the method illustrated in Fig. 3b. We hypothesize the following scaling form for τ

$$\tau = L^z f[(P_x - P_{xc})L^{z/\nu}], \quad (1)$$

which predicts that a crossing will appear with increasing sizes when plotting τ/L^z versus P_x . We see consistent results with this scaling assumption in Fig. 3b, from which we locate $P_{xc} = 0.72(1)$. A similar analysis was used for other values of $P \neq 0.15$ to extract the phase diagram in Fig. 2a. After locating P_{xc} , we then collapse the data as shown in the inset to Fig. 3b to obtain an estimate $\nu = 1/2$, which is also consistent with the prediction from mean-field percolation. We leave a more detailed analysis of the critical properties of this model for future work.

Data availability

All data is available in the manuscript or the Supplementary Information.

References

32. Maslov, D. Basic circuit compilation techniques for an ion-trap quantum machine. *N. J. Phys.* **19**, 023035 (2017).

Acknowledgements

We acknowledge fruitful discussions with E. Altman, S. Choi, A. Deshpande, S. Diehl, B. Fefferman, S. Gopalakrishnan, M. Ippoliti, V. Khemani, A. Nahum, J. Pixley, O. Shtanko and A. Zabalo, and the contributions of M. Goldman, K. Beck, J. Amini, K. Hudek and J. Mizrahi to the experimental set-up. This work is supported by the ARO through the IARPA LogiQ programme, the NSF STAQ programme, the AFOSR MURI on Dissipation Engineering in Open Quantum Systems and Quantum Measurement/Verification and Quantum Interactive Protocols, the ARO MURI on Modular Quantum Circuits, the DoE Quantum Systems Accelerator, the DoE ASCR Accelerated Research in Quantum Computing programme (award no. DE-SC0020312) and the National Science Foundation (QLCI grant no. OMA-2120757). L.E. is also funded by NSF award no. DMR-1747426. This work was performed at the University of Maryland with no material support from IonQ.

Author contributions

C.N. collected the data. C.N. and P.N. analysed the data. C.N., P.N. and M.J.G. wrote the manuscript and designed figures. M.C. and C.M. led construction of the experimental apparatus with contributions from C.N., D.Z., A.R., L.E. and D.B. Theory support was provided by P.N., M.J.G., A.V.G. and D.A.H. C.M., M.J.G. and D.A.H. supervised the project. All authors discussed the results and contributed to the manuscript.

Competing interests

The authors declare no competing interests.

Additional information

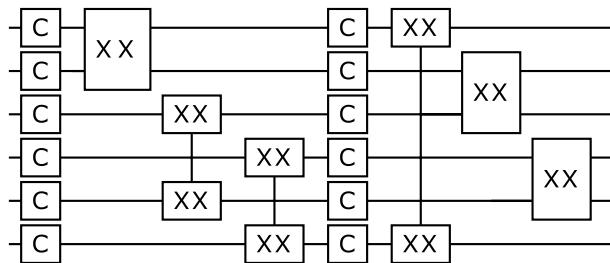
Extended data is available for this paper at <https://doi.org/10.1038/s41567-022-01619-7>.

Supplementary information The online version contains supplementary material available at <https://doi.org/10.1038/s41567-022-01619-7>.

Correspondence and requests for materials should be addressed to Crystal Noel.

Peer review information *Nature Physics* thanks Yi-Zhuang You and Tobias Schaetz for their contribution to the peer review of this work.

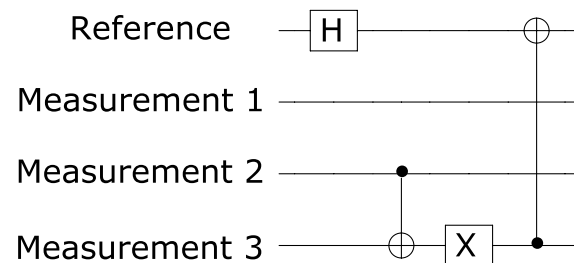
Reprints and permissions information is available at www.nature.com/reprints.



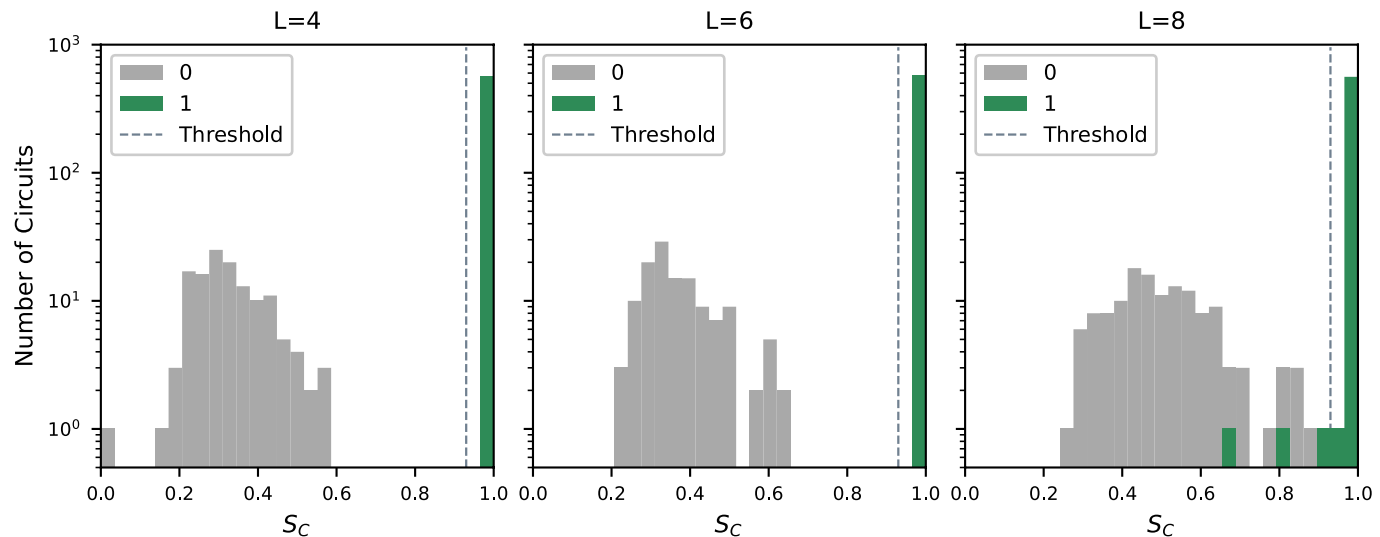
Extended Data Fig. 1 | Scrambling Unitary. Example of a scrambling unitary on a system with $L = 6$ qubits. Each single-qubit gate C refers to a random single-qubit Clifford gate. The XX gates have an implied rotation angle of $\pi/4$.

Measurement Record	Reference State
001	0
010	
101	
110	
000	1
011	
100	
111	

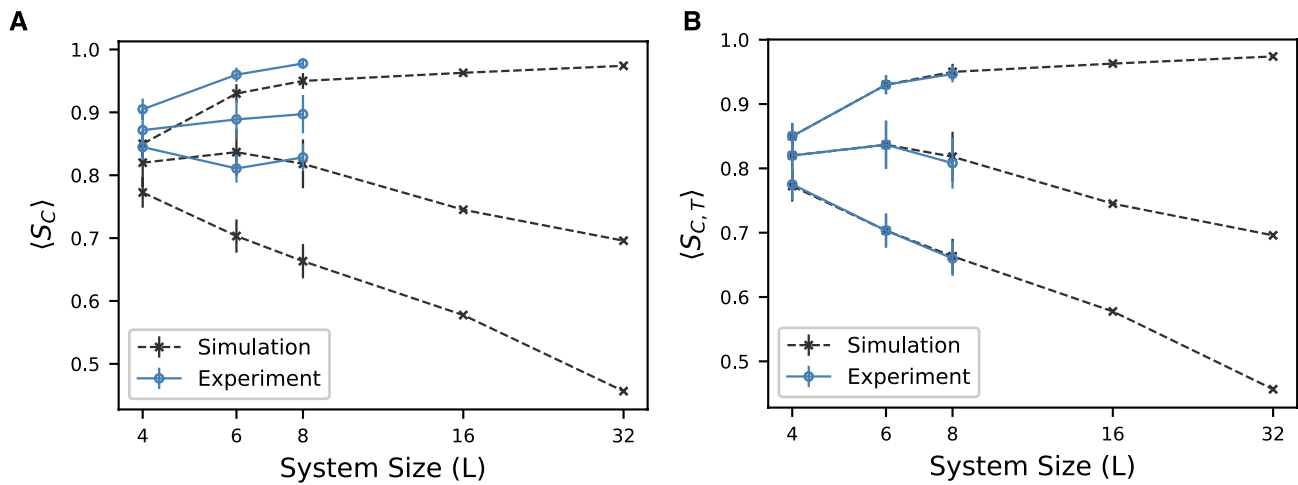
Extended Data Fig. 2 | Feedback Truth Table. Truth table for outcomes of measurement ancillae and reference qubit for a circuit.



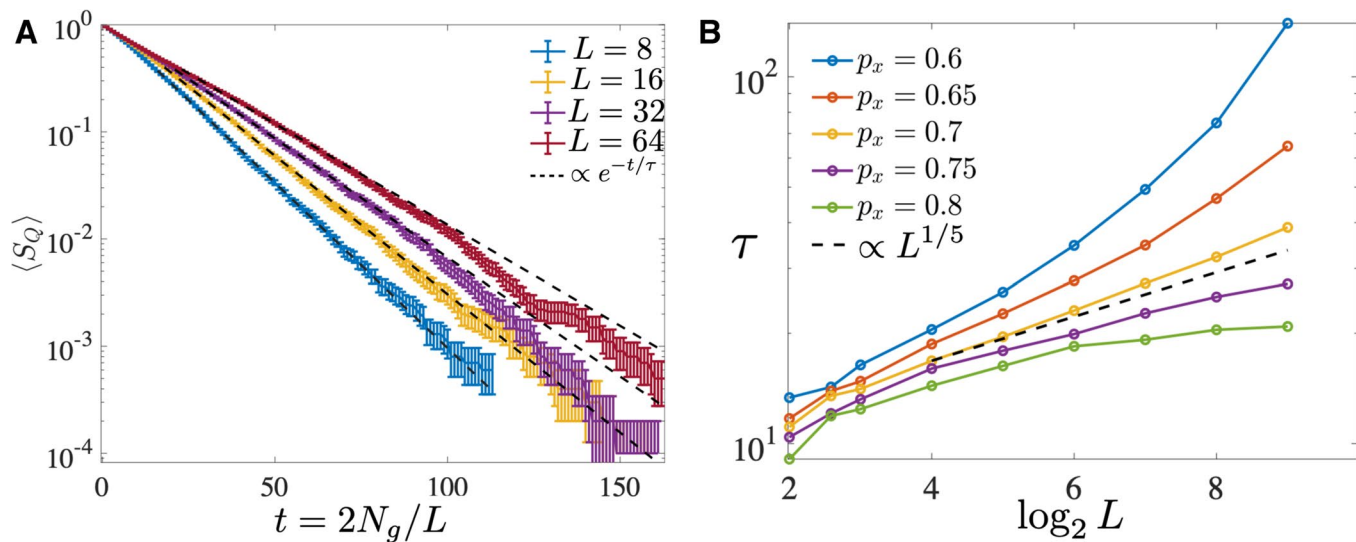
Extended Data Fig. 3 | Feedback Circuit. Feedback circuit corresponding to example circuit #45 described in Methods.



Extended Data Fig. 4 | Histogram of Experimental Data for S_C. All raw outcomes of S_C in study of phases (main text Fig. 3a). The legend indicates the simulated expected outcome for that circuit. The bin size is .033 and $S_C = .93$ (dashed line) is used as a threshold for all the data.



Extended Data Fig. 5 | Comparison of Theory and Experiment. **(a)** Raw average of all circuit outcomes without thresholding applied. **(b)** Thresholded data with extended simulations showing expected behaviour up to $L=32$.



Extended Data Fig. 6 | Analysis Method to Extract Critical Data. (a) Late time decay of $\langle S_Q \rangle$ showing the exponential decay regime used to extract the decay rate τ . Here, we took $(P, P_x) = (0.15, 0.7)$ near the critical point. (b) Scaling of τ vs L for different values of P_x at $P = 0.15$. We can estimate P_{xc} and extract z by looking for the inflection point in this family of curves and fitting the slope.